



POTSDAM-INSTITUT FÜR
KLIMAFOLGENFORSCHUNG

Originally published as:









Ma, R., Zhang, Y., Yang, Z., [Kurths, J.](#), Zhan, M., Lin, C. (2023): Synchronization stability of power-grid-tied converters. - Chaos, 33, 3, 032102.

DOI: <https://doi.org/10.1063/5.0136975>

REVIEW ARTICLE | MARCH 16 2023

Synchronization stability of power-grid-tied converters

Special Collection: [Disruption of Networks and System Dynamics](#)

Rui Ma ; Yayao Zhang  ; Ziqian Yang ; Jürgen Kurths ; Meng Zhan  ; Congping Lin 



Chaos 33, 032102 (2023)

<https://doi.org/10.1063/5.0136975>



View
Online



Export
Citation

CrossMark

AIP Advances

Why Publish With Us?



25 DAYS
average time
to 1st decision



740+ DOWNLOADS
average per article



INCLUSIVE
scope

[Learn More](#)

Synchronization stability of power-grid-tied converters

Cite as: Chaos 33, 032102 (2023); doi: 10.1063/5.0136975

Submitted: 30 November 2022 · Accepted: 24 February 2023 ·

Published Online: 16 March 2023



View Online



Export Citation



CrossMark

Rui Ma,¹  Yayao Zhang,¹  Ziqian Yang,²  Jürgen Kurths,^{3,4}  Meng Zhan,^{1,a)}  and Congping Lin⁵ 

AFFILIATIONS

¹State Key Laboratory of Advanced Electromagnetic Engineering and Technology, Hubei Electric Power Security and High Efficiency Key Laboratory, School of Electrical and Electronic Engineering, Huazhong University of Science and Technology, Wuhan 430074, China

²China Southern Power Grid Electric Power Research Institute (SEPRI), Guangzhou 510080, China

³Potsdam Institute for Climate Impact Research, Potsdam 14473, Germany

⁴Institute of Physics, Humboldt University Berlin, Berlin 12489, Germany

⁵School of Mathematics and Statistics and Center for Mathematical Sciences, Hubei Key Lab of Engineering Modeling and Scientific Computing, Huazhong University of Science and Technology, Wuhan 430074, China

Note: This paper is part of the Focus Issue on Disruption of Networks and System Dynamics.

^{a)}**Author to whom correspondence should be addressed:** zhanmeng@hust.edu.cn

ABSTRACT

Synchronization stability is one of central problems in power systems, and it is becoming much more complicated with the high penetration of renewable energy and power electronics devices. In this paper, we review recent work by several nonlinear models for renewable-dominated power systems in terms of multiple timescales, in particular, grid-tied converters within the DC voltage timescale. For the simplest model, a second-order differential equations called the *generalized swing equation* by considering only the phase-locked loop (PLL) is obtained, which shows a similar form with the well-known swing equation for a synchronous generator in the traditional power systems. With more outer controllers included, fourth-order and fifth-order models can be obtained. The fourth-order model is called the *extended generalized swing equation*, exhibiting the combined function of grid synchronization and active power balance on the DC capacitor. In addition, a nonlinear model for a two coupled converter system is given. Based on these studies, we find that the PLL plays a key role in synchronization stability. In summary, the value of this paper is to clarify the key concept of the synchronization stability in renewable-dominated power systems based on different nonlinear models, which still lacks systematic studies and is controversial in the field of electrical power engineering. Meanwhile, it clearly uncovers that the synchronization stability of converters has its root in the phase synchronization concept in nonlinear sciences.

Published under an exclusive license by AIP Publishing. <https://doi.org/10.1063/5.0136975>

With fast integration of renewable energy and development of power electronic technology, the traditional power system composed of the synchronous generator (SG) is gradually changing into the new-generation power system dominated by renewable energy and power electronic apparatuses. This greatly changes the power system dynamic performance and consequently all aspects of power systems, including analysis, relaying, control, and operation. Accidents induced by renewables have been reported around the world in the past few decades, severely threatening the safety of our modern power systems. Different from the SG whose characteristics have been well mastered in the past 100 years, the

characteristics of renewable energy equipment remain unclear, including the most important synchronization property. Recognizing that the synchronization stability of renewable-dominated power systems has become a very hot topic in the field of power electrical engineering, and meanwhile, unfortunately, there are few relevant reports in the field of physics; this paper aims to clarify its multi-timescale property by introducing several nonlinear models. It is expected to stimulate general interest of researchers who work on either renewable integration stability in power electrical engineering or a synchronization problem in nonlinear dynamics.

I. INTRODUCTION

The phenomenon of (phase) synchronization was first reported by Christian Huygens in 1665 when he observed that two pendulum clocks suspended on a beam swung antiphase with the same frequency.^{1,2} Nowadays, synchronization has been widely found in natural systems, social systems, and engineering practices, and the synchronization concept has also been greatly extended.² It plays a crucial role in system functions in many coupled element systems, and it has become one of the central problems in multidisciplinary fields. In power grids, synchronization between all AC electrical devices is necessary. Synchronization stability (or termed as rotor-angle stability) is a prerequisite for power system operation, among with other two types of stability (voltage stability and frequency stability). It is one of the central problems in modern power systems.^{3,4}

In the traditional power systems dominated by synchronous generators (SGs), the synchronizing process is determined by the dynamical characteristics of SGs, which are driven by the imbalance power between the input electromechanical power and the output electromagnetic power on their rotors. The synchronization stability is determined by the mutual motion of the rotors. Under this situation, the electromechanical timescale dynamics is dominant. Therefore, in the classical model of power systems, the system dynamics can be simplified and described by a model of coupled second-order Kuramoto phase oscillators.³⁻⁷ For the (nonlinear) transient stability analyses, numerical and analytical methods have been developed and investigated.⁸⁻¹⁰ In addition, the power grid synchronization has also been widely studied in the field of complex systems. For instance, the bifurcation phenomena of SG have been explored on the second-order and third-order models and considering the effect of stochastic fluctuations.¹¹⁻¹⁴ The synchronization stability conditions and cascading failures have been studied in some realistic systems based on the second-order Kuramoto oscillators.¹⁵⁻¹⁸ A novel concept of basin stability has been proposed to evaluate the impact of network topology on the synchronization stability.^{19,20} Small vulnerable sets, which lead to cascading failures, have been identified in the North American power grid.²¹ Besides, self-organized criticality of synchronization has also been studied.^{22,23}

Recently, increasing clean energy has been integrated into power grids by diverse renewable energy devices, mainly including a double-fed induction generator (DFIG) and a permanent magnetic synchronous generator (PMSG) for the wind energy and a photovoltaic (PV) generator for the solar energy.²⁴⁻²⁶ These generators relying on power electronic devices have been gradually substituting the major position of SGs, and this is generally believed as the second revolution of power systems. The wind and PV generations widely use multi-timescale controllers; e.g., the AC current controller typically has the shortest time constant (around 10 ms), the DC voltage controller has a medium time constant (around 100 ms), and the mechanical speed controller has the longest electromechanical time constant (around 1000 ms). Therefore, different from the dominant electromechanical dynamics of SG in the synchronization stability, not only electromechanical dynamics but also electromagnetic dynamics has to be considered. To make it worse, some switching controllers should be included during faults. In addition, comparatively, the energy density of renewables is much smaller. Usually hundreds of wind turbines are integrated in a wind farm and then

connected to power grids, tremendously increasing the spatiotemporal complexities. For a much longer timescale, the intermittency and fluctuation of renewables should be further studied. Just due to these intrinsic properties, we, human being, have not fully handled them yet. In the last few decades, synchronous instability accidents due to renewable energy with an unknown mechanism have been continuously reported around the world.²⁷⁻³⁰ Therefore, it is urgent to uncover the synchronization mechanism for the new-generation power systems.

Indeed, it has attracted broad interest of researchers in the field of power electrical engineering recently. Several methods have been applied and extended, including the time-domain simulation,³¹ the energy function (or the Lyapunov function) method,³² equal area criterion analysis,³³⁻³⁶ etc. Some nonlinear techniques, e.g., bifurcation analysis,³⁷⁻³⁹ phase portrait,⁴⁰ and basin of attraction,^{41,42} have been used to study the large-signal stability of grid-tied converters under different faults, especially, voltage dips. Meanwhile, the method of an amplitude/frequency motion equation has been proposed to analyze the relation between the apparatus and system transient responses.^{43,44} In addition, the synchronization with 100% renewable energy has also been proposed and studied.⁴⁵⁻⁴⁸ For more details, see some recent reviews and references therein.⁴⁹⁻⁵⁴

In this paper, we focus on the grid-tied converter as a key component of any grid-tied renewable devices and review recent progresses in its synchronization stability problem of renewable-energy-dominated power systems from the perspective of multi-timescale properties. Based on several nonlinear models of converters, it is found that the phase-locking loop (PLL) plays a key role in synchronization stability, and the PLL output angle plays a similar role of a rotor angle in traditional power systems. It also performs a close connection with the phase synchronization concept in nonlinear sciences. Comparing with the PLL, the active and reactive power branches play a secondary and tertiary role in the synchronization of converters, which is quite distinct from the SG. The remainder of this paper is structured as follows. First, in Sec. II, by focusing on the DC voltage timescale dynamics, the synchronous model (termed as the generalized swing equation) is established and studied when the PLL dynamics is considered solely. It is expected to play a similar role with the swing equation in the traditional power systems. Then, in Sec. III, two higher-order models are derived by including the outer controls of the active and reactive power branches. The fourth-order equations have the combined function of synchronization and power balance. Thus, the hierarchical relation becomes clear. In Sec. IV, the synchronization dynamical equations for two coupled converters are given, which are comparable to the coupled Kuramoto phase oscillator equations. Finally, conclusion and discussions are addressed in Secs. V and VI, respectively.

II. SYNCHRONIZATION DYNAMICS OF A SYNCHRONOUS CONTROL LOOP

In a wind farm, (kinetic) wind energy is converted to electromagnetic power by wind turbines and power electronic equipment. Usually, hundreds of wind turbines are integrated to the hub line and then connected to a high-voltage grid through the boost transformer, as schematically shown in Fig. 1. Generally, the connecting structure can be radical, radical-loop, or star-like. In the

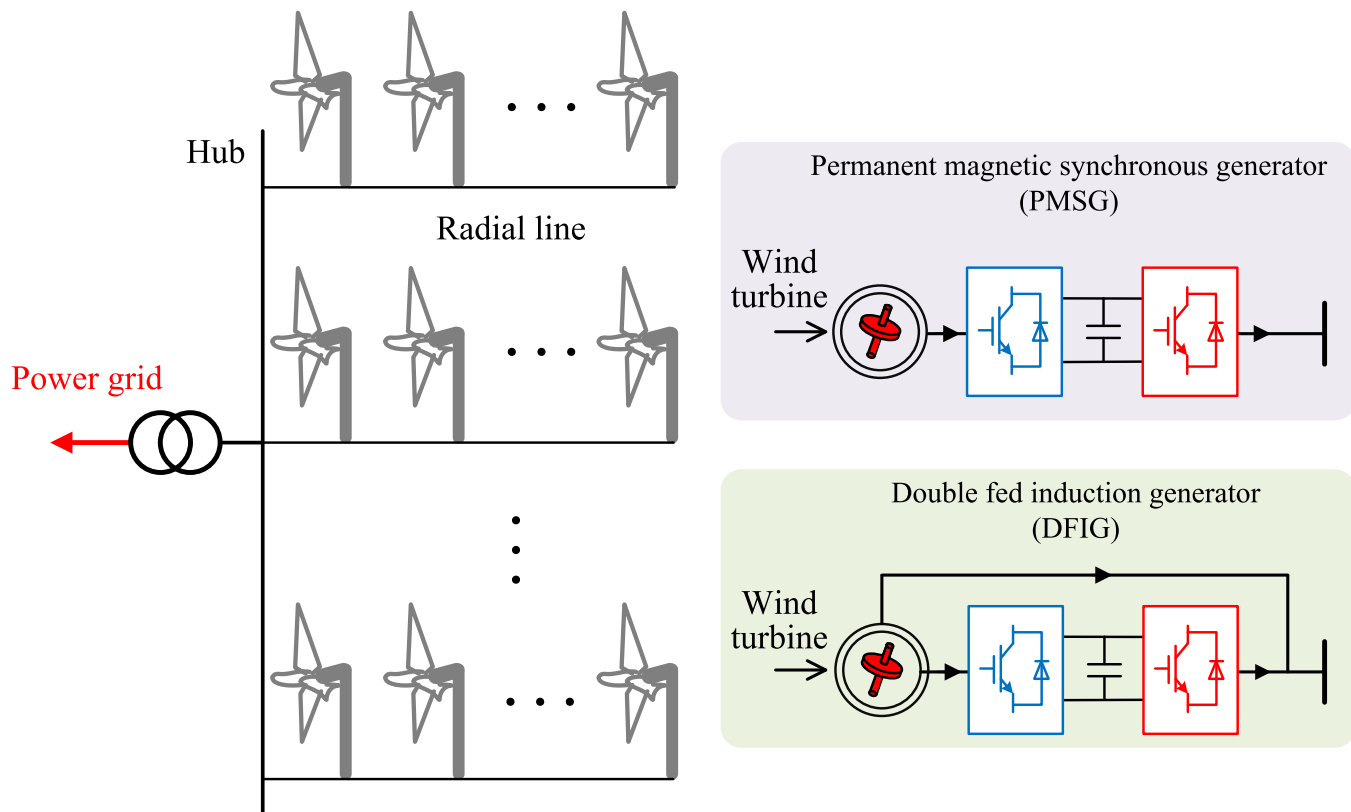


FIG. 1. Schematic shows of a wind farm consisting of wind generators and the two typical wind generators, including the permanent magnetic synchronous generator (PMSG) and the double-fed induction generator (DFIG). Usually, hundreds of wind turbines are integrated in a wind farm in a very wide area and then connected to power grids.

engineering practice, there are two types of wind turbines, a double-fed induction generator (usually termed as type III) and a permanent magnetic synchronous generator (termed as type IV), as shown in the right of Fig. 1.²⁶ In particular, the main control structures of the PMSG are illustrated in detail in Fig. 2. For any renewable energy integration, a three-phase voltage source converter (VSC) is adopted as the grid interface (as emphasized the “grid-side VSC” part in Fig. 2), and it plays a key role in the system dynamics. Generally, the grid-side VSC synchronizes with the power grid through either grid-following (GFL) or grid-forming (GFM) controls. The GFL strategy is realized based on the PLL. For the GFM control, which includes a virtual synchronous generator, droop, and power synchronization controls, etc.,^{50,55} it is believed as capable of providing grid-supporting capability through simulating the SG features.^{56,57} Compared with the GFM control, the GFL control is dominant in the engineering practice currently. Therefore, in this paper, we will mainly focus on the synchronization stability of the PLL-based VSC.

A. Nonlinear modeling

As one example, Fig. 2 schematically shows the control structures of the PMSG and the generator-side VSC (the lower left part) and the grid-side VSC (the lower right part).⁵⁸ As we concentrate

on the DC voltage timescale, we will mainly study the grid-side VSC and ignore the dynamics of the generator-side VSC completely. Under this situation, a constant power input is assumed; i.e., the output power of the generator-side VSC (or, equivalently, the input power of the grid-side VSC) is treated as a constant; $P_{in} = constant$. The grid-side VSC is connected to the AC grid through a filter inductance L_f , and the grid inductance is denoted by L_g . The PLL (emphasized by the red dotted box in Fig. 2) provides the dq synchronous frame to synchronize with the AC grid by inputting the three-phase terminal voltages of VSC (u_{tabc}) and then outputting the PLL phase, θ_{pll} . Here, we use u_{tabc} to denote the three-phase terminal voltages in the stationary reference, u_{ta} , u_{tb} , and u_{tc} . In addition, there are inner and outer controllers. For the outer controller, the direct voltage control (DVC) generates the d -axis current references i_{dref} to maintain the DC voltage constant, and the terminal voltage control (TVC) generates the q -axis current references i_{qref} to regulate the terminal voltage. Meanwhile, for the inner loop, the alternative current control (ACC) generates the reference voltage e_{dq} according to the current reference from the outer controllers. Finally, six insulated gate bipolar translators are driven by the modulated signals of reference voltages to produce the VSC output voltage e_{abc} through the technique of the pulse-width modulation.⁵⁹

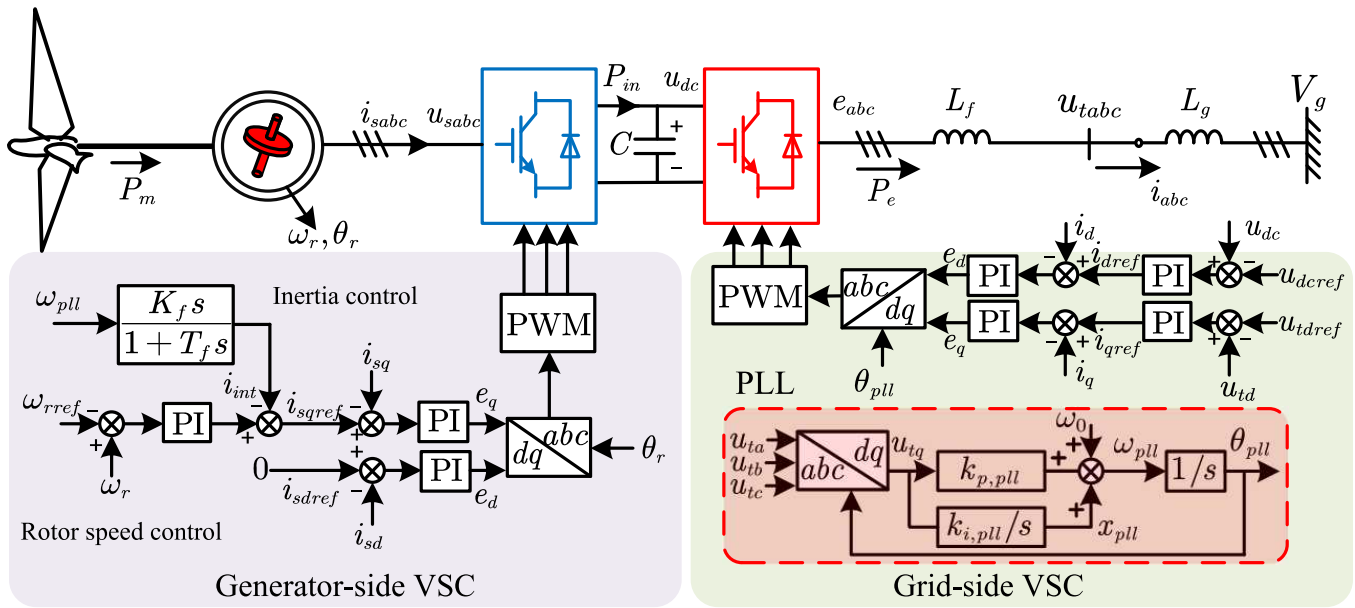


FIG. 2. Main control structures of the PMSG. Besides the PLL for synchronization (emphasized by a dashed-line box within the grid-side VSC), there are normally the ACC, DVC, and TVC in the grid-side VSC and the inertia and rotor speed controls in the generator-side VSC. In a transient process, some other transient controls should be considered.

As the PLL dynamics is much slower than that of the ACC,^{38,39,60,61} we assume that the output currents instantaneously track their references; i.e., $i_d = i_{dref}$ and $i_q = i_{qref}$. In addition, as the first step of simplification, we can assume that the outputs of voltage controls are constant; i.e., $i_{dref} = constant$ and $i_{qref} = constant$, based on the fact that the dynamic behavior of the PLL is usually faster than that of the voltage control loops. This is also correct under some particular conditions, such as a low voltage ride through. Under these simplified conditions, it is reasonable to start from the second-order model for the PLL control,^{32–36,41}

$$\begin{cases} \dot{\theta}_{pll} = \int (x_{pll} + k_{p,pll}u_{tq} + \omega_0) dt, \\ \dot{x}_{pll} = \int k_{i,pll}u_{tq} dt, \end{cases} \quad (1)$$

where $k_{p,pll}$ and $k_{i,pll}$ represent the proportional and integral coefficients of the PLL control, respectively, ω_0 the synchronous (working) frequency of the grid, x_{pll} the integral output of the PLL, and u_{tq} the q -axis component of the three-phase terminal voltage u_{tabc} . Consequently, we have $\omega_{pll} = \dot{\theta}_{pll} = x_{pll} + k_{p,pll}u_{tq} + \omega_0$.

For the relation between the terminal voltage V_t ($V_t = u_{td} + ju_{tq}$), the infinite bus voltage V_g ($V_g = V_g \cos \varphi - jV_g \sin \varphi$), and the VSC current output I_{vsc} ($I_{vsc} = i_d + ji_q$), we have

$$V_t = V_g + j\omega_{pll}L_g I_{vsc}, \quad (2)$$

which yields

$$\begin{cases} u_{td} = -\omega_{pll}L_g i_{qref} + V_g \cos \varphi, \\ u_{tq} = \omega_{pll}L_g i_{dref} - V_g \sin \varphi, \end{cases} \quad (3)$$

where $\varphi = \theta_{pll} - \omega_0 t$. The infinite bus V_g always works as a fixed voltage source with a constant amplitude V_g and a working frequency ω_0 . Note that $V_t = V_g + j\omega_0 L_g I_{vsc}$ has also been used in the literature. The schematic show for a grid-connected VSC system and the associated coordinates for the PLL dq frame (with a rotating speed ω_{pll}) and the synchronous xy frame (with a fixed rotating speed ω_0) and their corresponding phase relations are given in Fig. 3. Here, within the synchronous xy frame, the PLL inputs the terminal voltage phase φ_t and outputs the phase φ . φ denotes the phase difference between the PLL dq frame and the synchronous xy frame, and φ_t denotes the terminal voltage phase in the synchronous xy frame. In the steady state, $\varphi = \varphi_t$.

After some algebraic derivations, we obtain the following equations for the synchronization phase difference:

$$M_{eq} \ddot{\varphi} = P_m - P_e - D_{eq}(\varphi) \dot{\varphi}, \quad (4)$$

where

$$\begin{cases} M_{eq} = \frac{1 - k_{p,pll} L_g i_{dref}}{k_{i,pll}}, \\ P_m = \omega_0 L_g i_{dref}, \\ P_e = V_g \sin \varphi, \\ D_{eq} = \frac{k_{p,pll}}{k_{i,pll}} V_g \cos \varphi - L_g i_{dref}. \end{cases} \quad (5)$$

Here M_{eq} , P_m , P_e , and D_{eq} denote equivalent inertia, mechanical power, electromagnetic power, and damping, respectively. Clearly, the equation shows certain similarities with the classical swing equation in the traditional power systems,^{3,4} $M\ddot{\varphi} = P_m - P_e - D\dot{\varphi}$, and thus, they can be referred to as a *generalized swing equation*. In addition, we find that for the steady-state solution, $\dot{\varphi} = 0$ ($\omega_{pll} = \omega_0$)

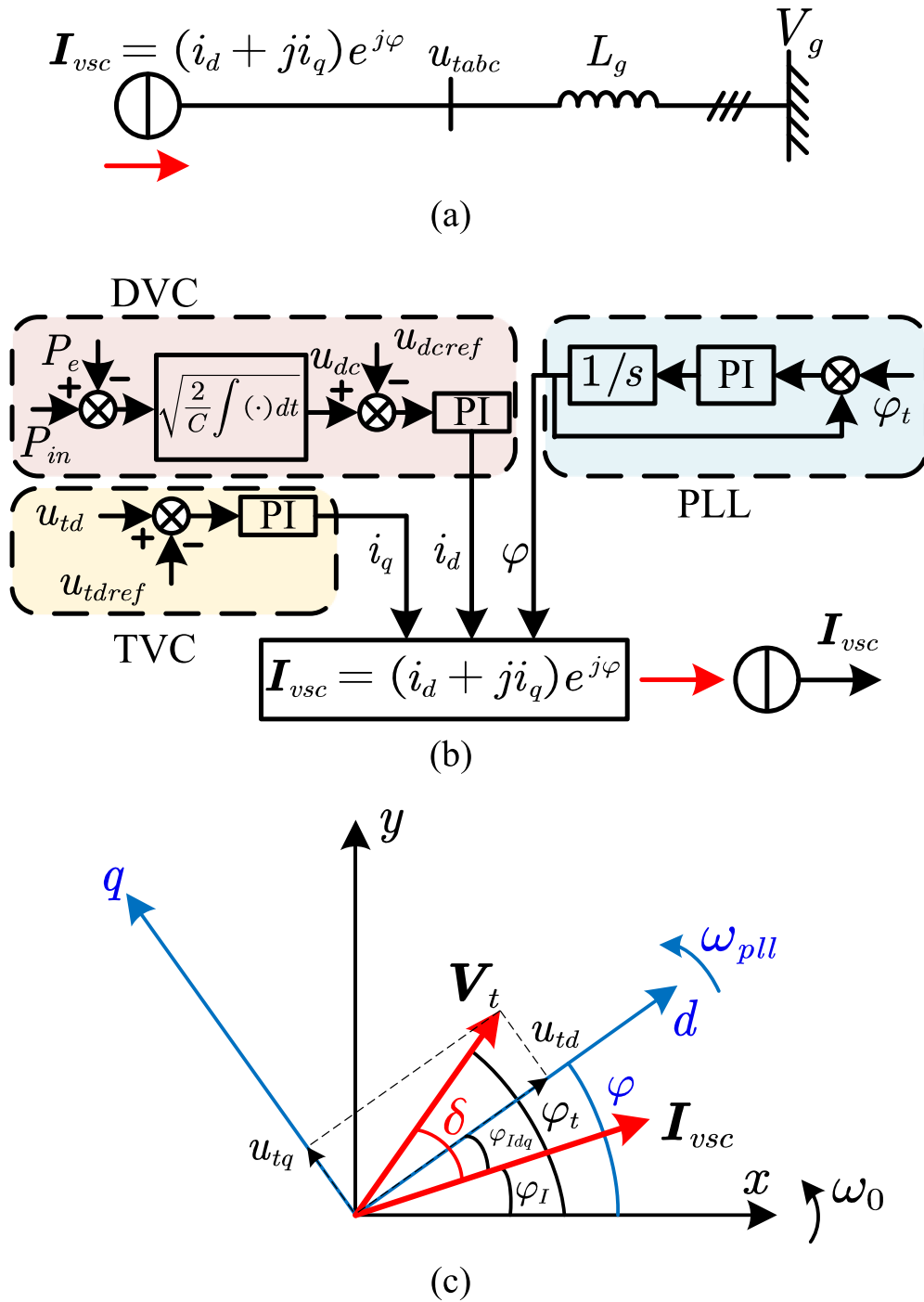


FIG. 3. (a) Within the DC voltage timescale, the converter can be treated as a controlled-current source, $\mathbf{I}_{vsc} = (i_d + ji_q)e^{j\varphi}$, within the synchronous reference frame. (b) Schematic show for the decomposition of the controller effects. With more branches considered (DVC for the active current and TVC for the reactive current), the system dynamics can be more correctly described. The PLL phase output φ (or its associated frequency ω_{pll}) is essential. $\varphi = \theta_{pll} - \omega_0 t$. (c) Schematic show for the relations of different coordinates and angles. φ denotes the phase difference between the PLL dq frame and the synchronous xy frame, φ_t denotes the terminal voltage phase in the synchronous xy frame, δ is the power factor angle between the current vector and the terminal voltage vector, and φ_{Idq} and φ_I are the current angle in the dq and xy frames, respectively.

and $\varphi = \text{constant}$, indicative of an identical frequency between the PLL output and grid, or phase synchronization between the PLL and the grid in the language of nonlinear dynamics. More details can be found in Ref. 35.

B. Nonlinear dynamical analysis

After nondimensionalizing the variable t by setting

$$\tilde{t} = \sqrt{\frac{k_{i,pll} V_g}{1 - k_{p,pll} L_g i_{dref}}} t, \tag{6}$$

we further obtain³⁵

$$\ddot{\varphi} = I - \sin \varphi - (\alpha \cos \varphi - D)\dot{\varphi}, \tag{7}$$

where

$$\begin{cases} I = \frac{\omega_0 L_g i_{dref}}{V_g}, \\ D = \frac{L_g i_{dref}}{V_g} \sqrt{\frac{k_{i,pll} V_g}{1 - k_{p,pll} L_g i_{dref}}}, \\ \alpha = \frac{k_{p,pll}}{k_{i,pll}} \sqrt{\frac{k_{i,pll} V_g}{1 - k_{p,pll} L_g i_{dref}}}. \end{cases} \tag{8}$$

In mathematics, it is simpler with only three independent combined parameters (I , α , and D), whereas the original equation (4) has many parameters. Specifically, parameter I denotes the dimensionless power that is determined by the operation point, such as L_g , V_g , and i_{dref} . Parameter D represents the constant part of the equivalent damping D_{eq} ($D_{eq} = \alpha \cos \varphi - D$), and it is relevant to not only the operation point, including L_g , V_g , and i_{dref} , but also the integral coefficient of the PLL, $k_{i,pll}$. Parameter α represents the other part of the equivalent damping D_{eq} and mainly relies on

the ratio of proportional and integral coefficients of the PLL; i.e., $k_{p,pll}/k_{i,pll}$. It can be seen that these three parameters are the functions of multiple initial parameters. In mathematics, it is reasonable to treat them as independent parameters and perform analyses. After these analyses, we can easily obtain the results for the initial parameters. Compared with the normalized swing equation,¹ i.e., $\ddot{\varphi} = I - \sin \varphi - D\dot{\varphi}$, the only difference is that here, the equivalent damping D_{eq} becomes $(\alpha \cos \varphi - D)$, which is time-varying. Its dynamical behavior in Eq. (7) has been well analyzed.³⁵ Three kinds of bifurcations are revealed, including the generalized saddle-node, sub-critical Hopf, and homoclinic bifurcations, which divide the whole parameter space into four regions I, II, III, and IV, as shown in Fig. 4(a). $\alpha = 0.7$ is chosen without losing generality.

- (1) Generalized saddle-node bifurcation. It is located at the critical value $I_c = 1$ in Fig. 4(a), which is illustrated by a dashed line, just corresponding to the existence of equilibrium points. Above the dashed line, no equilibrium point exists.
- (2) Sub-critical Hopf bifurcation. It occurs at

$$I = \sqrt{1 - (D/\alpha)^2}, \tag{9}$$

- which indicates that two conjugate complex eigenvalues come across the imaginary axis in the linearized eigenvalue space. This bifurcation line intersects with the horizontal axis at $D = \alpha$. Within region III, two unstable equilibrium points coexist. Within region II, one stable equilibrium point, one unstable equilibrium point, and one unstable limit cycle coexist.
- (3) Homoclinic bifurcation. As D decreases, the stable manifold of the unstable equilibrium point collides with the limit cycle, indicative of a homoclinic bifurcation, illustrated by a dot-dashed line in Fig. 4(a). This bifurcation line is numerically

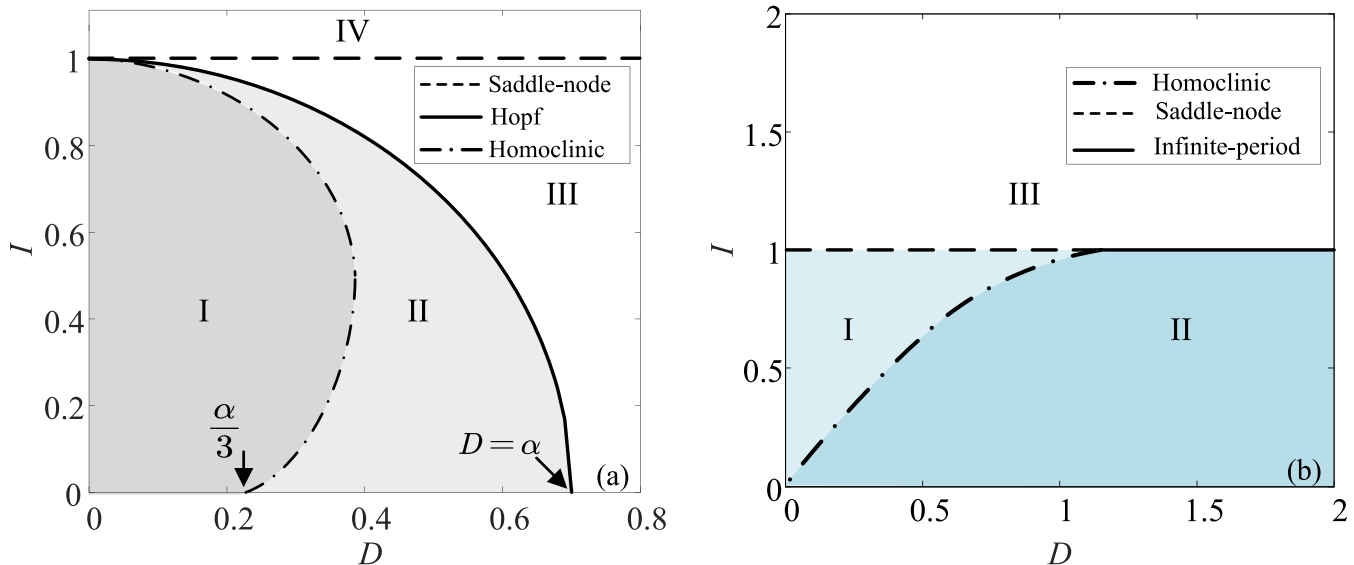


FIG. 4. Phase diagrams for the generalized swing equation (a) and the classical swing equation (b). In (a), $\alpha = 0.7$. Within the different parameter regions, the dynamics can be completely different. For more details, see the text.

obtained. At $I = 0$, the homoclinic bifurcation point at $D = \alpha/3$ can be theoretically estimated by the classical Melnikov method.

For comparison, the phase diagram for the swing equation is given in Fig. 4(b). Refer to any classical textbook on nonlinear dynamics, e.g., Ref. 1, for more details. In the swing equation, there only exists two parameters, i.e., I and D . Correspondingly, for the generalized swing equation, we also plot the bifurcation diagram on the I - D plane for a fixed α ($\alpha = 0.7$). For other values of α , the bifurcation diagram is similar.

As the generalized swing equation is essential for the dynamic performance of the grid-tied VSC, there are a large number of works on this equation. For example, several methods have been developed by neglecting the state-dependent damping term D_{eq} , such as the equal area criterion, the Lyapunov method, energy function methods, etc.³²⁻³⁶ Additionally, some numerical methods have been proposed, e.g., the methods of sum-of squares, estimates of basin of attraction, etc.^{41,42,62} More than stability analysis, engineers are also interested in transient stability assessment, stability enhancement, stability control, etc.

C. A model based on active and reactive powers

So far, we have obtained the simplest model of the PLL-based VSC, which can be treated as a controlled-current source with a phase output variable φ and two constant current references ($i_d = i_{dref}$ and $i_q = i_{qref}$) on the PLL coordinate, as schematically shown in Fig. 3(b), where it inputs the terminal voltage phase φ_t and outputs the PLL phase φ . Actually, we can also change the control diagram of the PLL slightly and make a connection with the power factor angle δ [$\delta = \arctan(Q/P)$]. $\varphi_t - \varphi = \delta - \varphi_{Idq}$ in Fig. 3(c). To be clearer, the original model and the modified model are schematically shown in Figs. 5(a) and 5(b), respectively. In the original model (top), there are two feedback loops, including φ and φ_t , from the outputs of the PLL and network, respectively, and their difference

$\varphi_t - \varphi$ is used as the input of the PLL. In contrast, the modified model (bottom) removes the inner feedback loop and makes the input-output relationship clearer. As the power factor angle φ depends on both active and reactive powers, it is more conducive to understanding synchronization from the perspective of power, with which power electric engineers are familiar. Refer to Ref. 46 for more details.

III. SYNCHRONIZATION DYNAMICS CONSIDERING OUTER CONTROLLERS

In Sec. II, the outputs of the outer voltage controls (i_{dref} and i_{qref}) in the simplified model are treated as constant. However, the DVC and TVC reflect the dynamical behaviors of active and reactive power imbalances, respectively, which might be non-negligible in some situations.^{38,63,64} In this section, two extended models are further established.

A. Incorporating active power branch

For the dynamics of the DC capacitor induced by the power imbalance,

$$d \frac{(1/2C_{dc}u_{dc}^2)}{dt} = P_{in} - P_e, \tag{10}$$

which can be rewritten as

$$\dot{u}_{dc} = \frac{1}{C_{dc}u_{dc}}(P_{in} - P_e), \tag{11}$$

where C_{dc} denotes the DC capacitor and u_{dc} represents its DC voltage. P_{in} and P_e separately denote the input and output powers. See the control structure in Fig. 2. For the DVC, the integral output x_{dvc} is chosen as the state variable,

$$\dot{x}_{dvc} = k_{i,dvc}(u_{dc} - u_{dcref}), \tag{12}$$

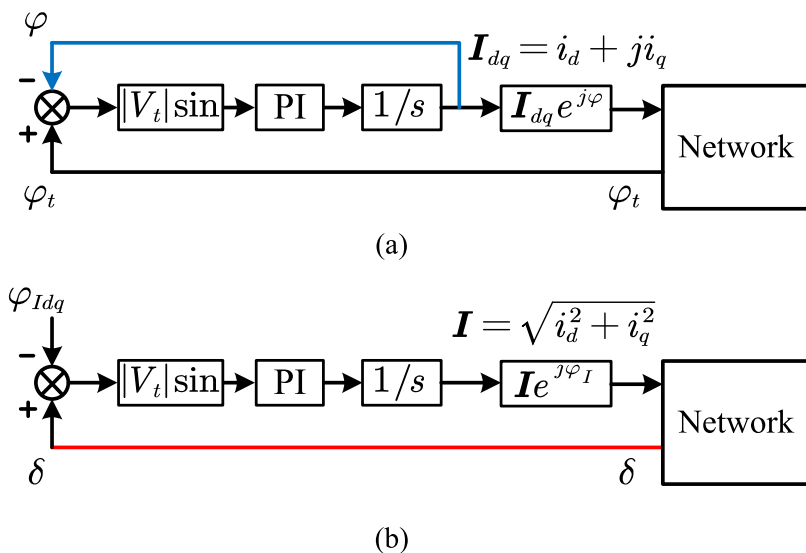


FIG. 5. Schematic diagram for the original model (a) and the modified model (b) for the PLL-based VSC system. In (a), there are two feedbacks, including the PLL output phase φ and the terminal voltage phase φ_t . In (b), there is only one feedback from the power factor angle δ , and hence, the relation becomes simple. In addition, it is connected with the active and reactive powers, which is more power-system-oriented. Here, we use $|U_t|$ to denote the terminal voltage amplitude.

where $k_{i,dvc}$ is the integral coefficient of the DVC. The output variable of the DVC, i_{dref} , can be obtained as

$$i_{dref} = k_{p,dvc}(u_{dc} - u_{dcref}) + x_{dvc}, \quad (13)$$

where $k_{p,dvc}$ denotes the proportional coefficient of the DVC.

When the PLL and the active power branch, including the DVC and DC capacitor dynamics, are considered, a fourth-order model is obtained,

$$\begin{cases} \dot{\varphi} = x_{pll} + k_{p,pll}u_{tq}, \\ \dot{x}_{pll} = k_{i,pll}u_{tq}, \\ \dot{u}_{dc} = \frac{1}{C_{dc}u_{dc}}(P_{in} - P_e), \\ \dot{x}_{dvc} = k_{i,dvc}(u_{dc} - u_{dcref}), \end{cases} \quad (14)$$

where u_{dc} represents the DC voltage, x_{dvc} denotes the integral output of DVC, and P_{in} and P_e separately denote the input and output powers on the DC capacitor, as shown in Fig. 2. The associated algebraic equations are

$$\begin{cases} u_{td} = 1, \\ u_{tq} = \omega_0 L_g i_{dref} - V_g \sin \varphi, \\ i_{dref} = k_{p,dvc}(u_{dc} - u_{dcref}) + x_{dvc}, \\ P_e = u_{td} i_{dref} + u_{tq} i_{qref}. \end{cases} \quad (15)$$

Then, φ_{tdq} is no longer a constant, and it becomes

$$\varphi_{tdq} = \arctan \frac{-i_q}{i_d(t)} = \arctan \frac{-i_q}{k_{p,dvc}(u_{dc} - u_{dcref}) + x_{dvc}}. \quad (16)$$

Clearly now, the VSC synchronization is realized by the PLL, which is depicted by the first two equations in Eq. (14), whereas for the power balance, it is achieved by the DVC and DC capacitor described by the last two equations in Eq. (14). The functions of synchronization (on the PLL) and power balance (on the DC

capacitor) are separate. In contrast, for the SG, the synchronization and the power balance are naturally integrated, which are uniformly reflected by the rotor motion dynamics and described by the well-known swing equation. In this respect, we may call the above fourth-order equations as *extended generalized swing equations*.

Numerical simulations are performed to validate the reduced order model. As shown in Fig. 6, the phase trajectories of the second-order, fourth-order, and full-order models are compared in different cases. Figures 6(a) and 6(b) separately illustrate the phase portraits based on different models when V_g dips to 0.8 pu (for a stable condition) and 0.3 pu (for an unstable condition). Compared to the second-order, the fourth-order model can capture the dynamic behaviors of the original model more accurately. Additionally, the synchronization issue is studied and shown in Fig. 7, where the terminal voltage angle (φ_t) and the PLL output angle (φ) are compared under these two different situations. In Fig. 7(a), when V_g dips to 0.8 pu, it can be seen that φ tracks φ_t well in the transient process. For this slight voltage dip, the PLL is able to maintain synchronous with the terminal voltage and the infinite bus. In contrast in Fig. 7(b), when V_g dips to 0.3 pu, the PLL can track the terminal voltage ($\varphi \approx \varphi_t$), while it cannot synchronize with the infinite bus as both φ and φ_t go to infinity. These dynamical behaviors are clearly similar to the phase synchronization (or phase-locking) in coupled oscillators.^{1,2}

B. Incorporating active and reactive power branches

When the integral output of the TVC (x_{tvc}) is chosen as the state variable, the dynamics of the TVC can be represented by

$$\dot{x}_{tvc} = k_{i,tvc}(u_{td} - u_{tdref}). \quad (17)$$

Similarly, the output variable of the TVC, i_{qref} , can be written as

$$i_{qref} = k_{p,tvc}(u_{td} - u_{tdref}) + x_{tvc}, \quad (18)$$

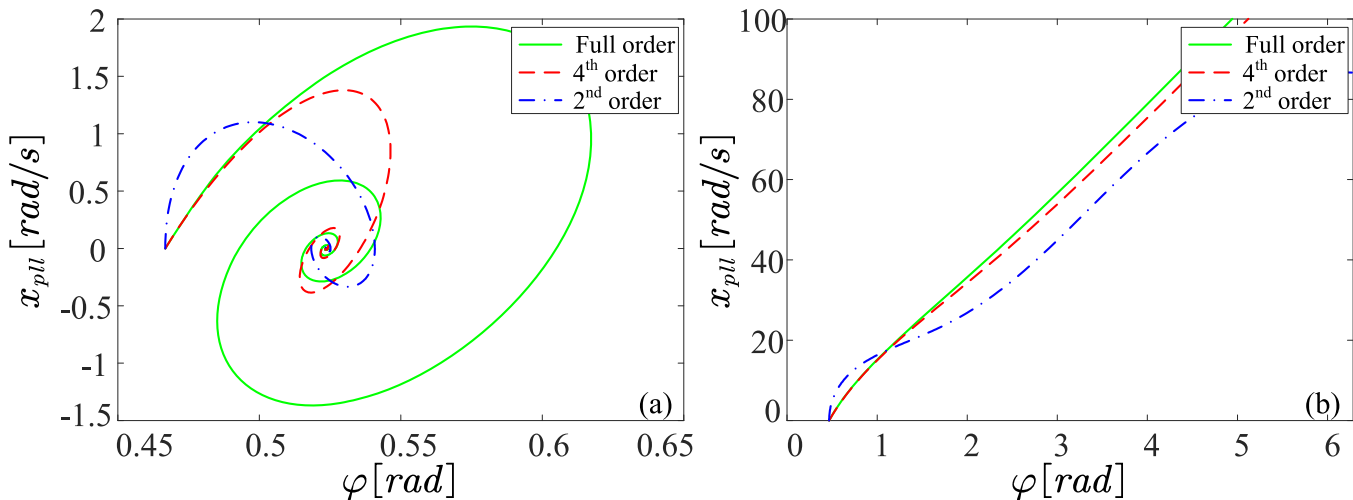


FIG. 6. Comparison of numerical results of the second-order, fourth-order, and full-order models for (a) a stable condition when V_g dips to 0.8 pu and (b) an unstable condition when V_g dips to 0.3 pu. The green solid, red dashed, and blue dotted-dashed lines represent the results of the full-order, fourth-order, and second-order models, respectively.

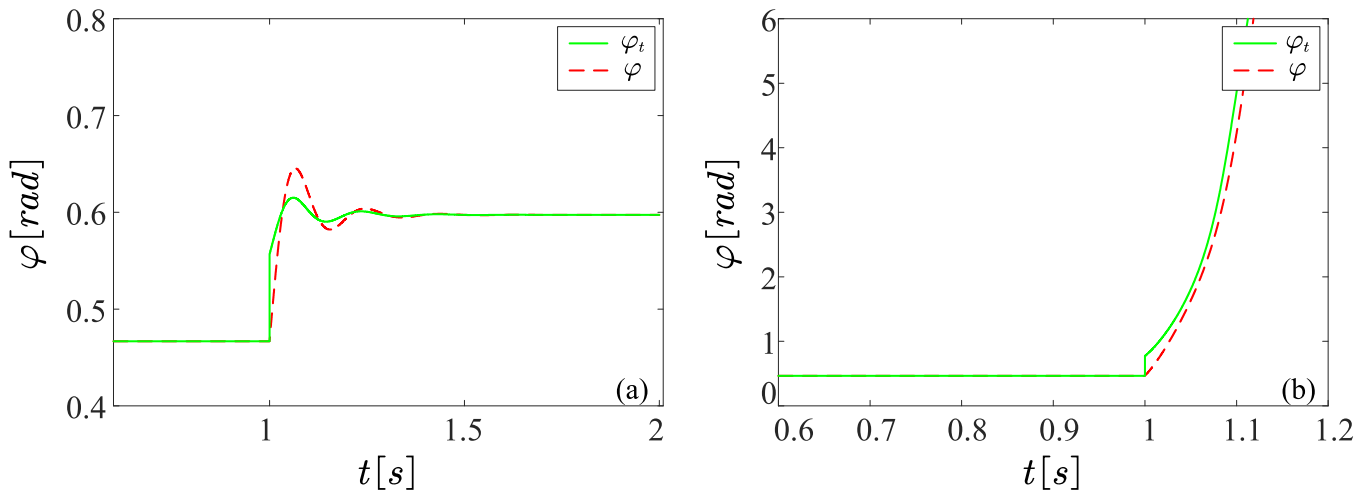


FIG. 7. Comparison of time series of the terminal voltage angle (φ_t) and the PLL output angle (φ) in the fourth-order model for (a) a stable condition when V_g dips to 0.8 pu and (b) an unstable condition when V_g dips to 0.3 pu. The green solid and red dashed lines represent φ_t and φ , respectively.

where $k_{i,dvc}$ and $k_{p,dvc}$ denote the integral and proportional coefficients of the DVC, respectively. Therefore, if we incorporate the reactive power branch, we obtain a fifth-order model,^{38,65}

$$\begin{cases} \dot{\varphi} = x_{pll} + k_{p,pll}u_{tq}, \\ \dot{x}_{pll} = k_{i,pll}u_{tq}, \\ \dot{u}_{dc} = \frac{1}{C_{dc}u_{dc}}(P_{in} - P_e), \\ \dot{x}_{dvc} = k_{i,dvc}(u_{dc} - u_{dcref}), \\ \dot{x}_{tvc} = k_{i,tvc}(u_{td} - u_{tdref}), \end{cases} \quad (19)$$

where x_{tvc} represents the integral output of the TVC. The algebraic equations are

$$\begin{cases} u_{td} = -\omega_0 L_g i_{qref} + V_g \sin \varphi, \\ u_{tq} = \omega_0 L_g i_{dref} - V_g \cos \varphi, \\ i_{dref} = k_{p,dvc}(u_{dc} - u_{dcref}) + x_{dvc}, \\ i_{qref} = k_{p,tvc}(u_{td} - u_{tdref}) + x_{tvc}, \\ P_e = u_{td} i_{dref} + u_{tq} i_{qref}. \end{cases} \quad (20)$$

Under this situation, by choosing the active and reactive power currents as inputs, φ_{tdq} becomes

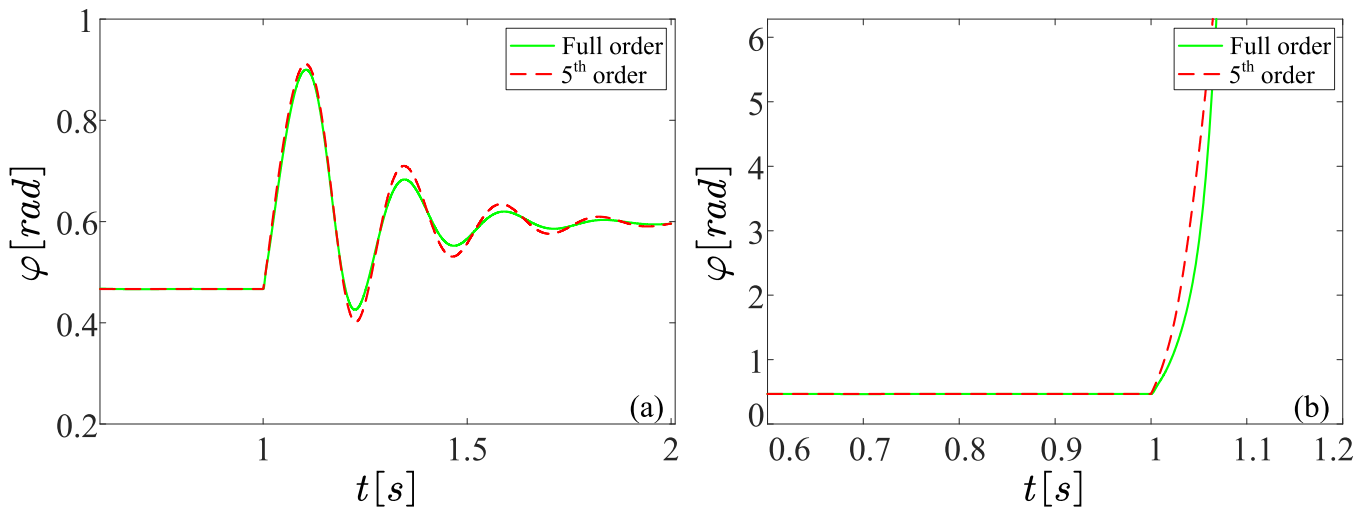


FIG. 8. Comparison of time series of the PLL output angle φ in the fifth-order and full-order models for (a) a stable condition when V_g dips to 0.8 pu and (b) an unstable condition when V_g dips to 0.3 pu. The green solid and red dashed lines are for the full-order and fifth-order models, respectively.

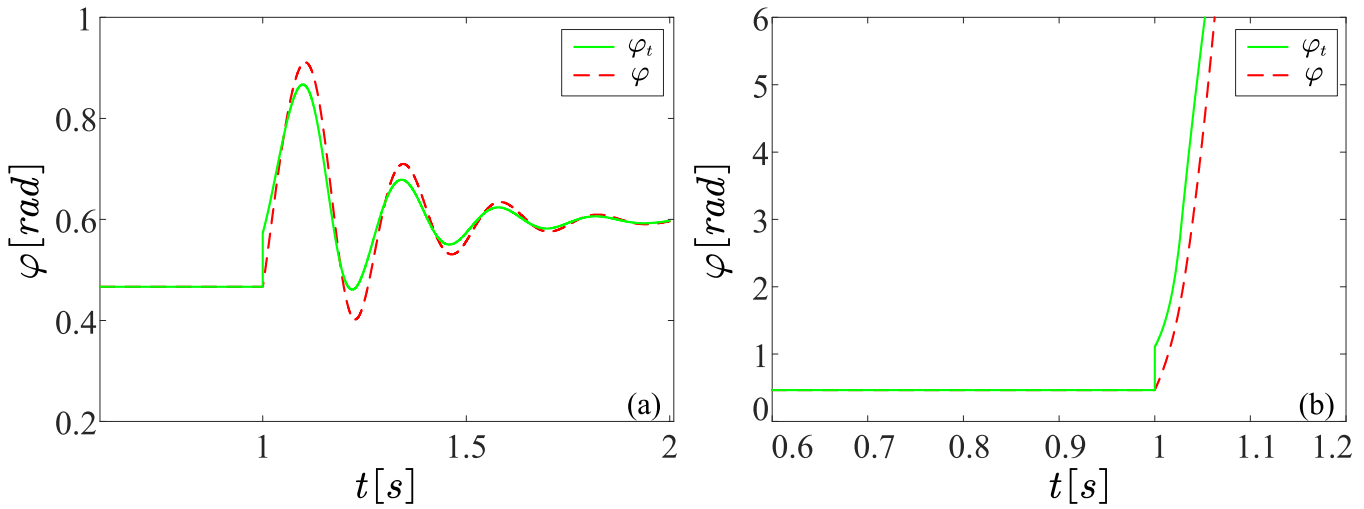


FIG. 9. Similar to Fig. 7, but for the fifth-order model, instead.

$$\varphi_{ldq} = \arctan \frac{-i_q(t)}{i_d(t)} = \arctan \frac{-k_{p,tvc}(u_{td} - u_{tdref}) - x_{tvc}}{k_{p,dvc}(u_{dc} - u_{dcref}) + x_{dvc}}. \quad (21)$$

Additionally, numerical simulations are conducted to verify the effectiveness of the reduced order model. As shown in Figs. 8(a) and 8(b), the time series of the fifth-order and full-order models are compared when V_g dips to 0.8 pu (for a stable condition) and 0.3 pu (for an unstable condition). One can see that no matter whether it is stable or unstable, the fifth-order model can accurately describe the dynamic behaviors of the full-order model. Meanwhile, the time series of the terminal voltage angle (φ_t) and the PLL output angle (φ) are shown in Fig. 9 correspondingly. Again, in the transient, the PLL output angle φ always tracks the terminal voltage angle φ_t for both the stable and unstable conditions ($\varphi \approx \varphi_t$). However, when V_g dips to 0.3 pu, the VSC suffers loss of synchronization with the infinite bus as both φ_t and φ go to infinity. The difference between the phase-locking and phase-unlocking in Figs. 9(a) and 9(b) is clear.

Clearly with the additive reactive power branch, this fifth-order model can catch the system dynamics within the DC voltage timescale more correctly. With this model, we have performed the transient stability analysis under a voltage dip and found some unusual phenomena, such as discontinuity of both amplitude and phase of the terminal voltage of VSC when the fault occurs or is clearer, and unusual multiple swings. Refer to Ref. 38 for more details.

IV. SYNCHRONIZATION DYNAMICS OF MULTIPLE CONVERTERS

With the above models for a single converter integration system, it is not difficult to develop similar models for multi-converter systems. However, we find that if the above fifth-order equations are used, the model is much complicated.⁶⁵ To be simple, take a model of two-parallel VSCs tied to an infinite bus considering only the PLL

dynamics as an example.⁶⁶⁻⁶⁹ The differential equations are then

$$M_i \ddot{\varphi}_i = P_{m,i}(\varphi_{ij}) - P_{e,i}(\varphi_i) - D_{eq,i}(\varphi_i) \dot{\varphi}_i - D_{c,i}(\varphi_{ij}) \dot{\varphi}_{ij}, \quad (22)$$

where $i, j = 1, 2$, φ_1 and φ_2 separately represent the phase differences between the dq frames of VSC1, VSC2 within the xy frame, and $\varphi_{ij} = \varphi_i - \varphi_j$. In addition,

$$\begin{cases} M_i = \frac{1}{k_{i,pll}}, \\ P_{m,i}(\varphi_{ij}) = \omega_0 (L_1 + L_g) i_{d,i} + \omega_0 L_g [i_{d,j} \cos(\varphi_{ij}) + i_{q,j} \sin(\varphi_{ij})], \\ P_{e,i}(\varphi_i) = V_g \sin \varphi_i, \\ D_{eq,i}(\varphi_i) = \frac{k_{p,pll}}{k_{i,pll}} V_g \cos \varphi_i, \\ D_{c,i}(\varphi_{ij}) = \frac{k_{p,pll} \omega_0 L_g}{k_{i,pll}} [i_{d,j} \sin(\varphi_{ij}) - i_{q,j} \cos(\varphi_{ij})], \end{cases} \quad (23)$$

where M , P_m , P_e , and D_{eq} still denote the equivalent inertia, mechanical power, electromagnetic power, and damping, respectively, and D_c represents the couplings between the two VSCs. The corresponding schematic show is given in Fig. 10. To be simple, the parameters

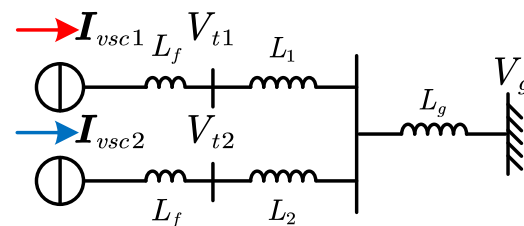


FIG. 10. Schematic show for a two-parallel VSC scenario.

of the two converters are chosen as identical. Basically, Eq. (22) is similar to the model of coupled Kuramoto phase oscillators.⁵ However, they are more complicated and difficult to analyze. Further studies are needed.

V. CONCLUSIONS

In conclusion, the synchronization stability in renewable-dominated power systems has been summarized based on the proposed multi-timescale models. In particular, the synchronization of grid-tied converters within the DC voltage timescale is focused. The generalized swing equation of the second-order model with only PLL considered and the extended generalized swing equation of the fourth-order model with both PLL and DVC are inferred. The whole system dynamics should be described by the fifth-order model with the PLL, DVC, and TVC. Therefore, within the DC voltage timescale, each converter can be treated as a controlled-current source, including the PLL output phase φ and the two current components within the dq coordinate established by the PLL, as illustrated in Fig. 3(b). If the slower electromechanical timescale dynamics is needed, the constant power input condition $P_{in} = constant$ should be released and the generator-side controls, such as the inertia and rotor speed controls, should be further considered; $P_{in} = P_{in}(t)$. The hierarchical structure and the organization rule have become clear. Based on these studies, we infer that the PLL output phase shows a similar contribution with the rotor angle of the SG, and the PLL plays a core role in the synchronization of the grid-tied converters and renewable devices as well. All these results

TABLE I. Hierarchical structure of grid-tied converters within the electromagnetic timescale for different control loops considered. Under this situation, $P_{in} = constant$, $i_d = i_{dref}$, and $i_q = i_{qref}$. With more outer controllers considered, more current dynamics should be studied. The electromechanical timescale dynamics under $P_{in} = P_{in}(t)$ should be further studied.

Control loop	Assumption
PLL	$i_d = i_{dref} = constant, i_q = i_{qref} = constant$
PLL + DVC	$i_d = i_{dref}(t), i_q = i_{qref} = constant$
PLL + DVC + TVC	$i_d = i_{dref}(t), i_q = i_{qref}(t)$

have been summarized in Fig. 11 and Table I. For power electrical engineers, this synchronization phenomenon might be the most beautiful symphony in the world.

VI. DISCUSSION

Finally, we emphasize some important points and unsolved problems for future works:

- (1) Although the synchronization stability of renewable-dominated power systems has been broadly studied in the field of power electrical engineering very recently, there is a heated and lively debate on the concept of synchronization stability. In the traditional power systems, the synchronization stability is equivalent to the rotor-angle stability, which is within the electromechanical timescale. The physical picture for this stability and/or instability determined by the mechanical motion on the power

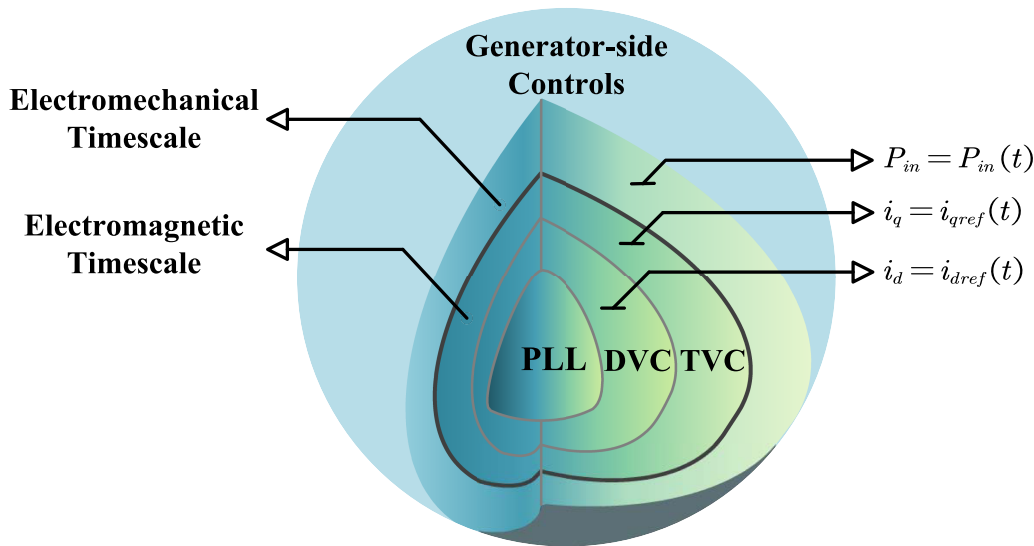


FIG. 11. Schematic show for the organization center of the synchronization stability of a grid-tied converter. Within the electromagnetic timescale denoted by a black solid curve, in the simplest form, it is described by the generalized swing equation within the electromagnetic timescale (~ 100 ms) with only the PLL considered. For a more precise dynamical description, the dynamics of TVC and DVC should be considered, which governs the dynamics of the current references i_{dref} and i_{qref} , respectively. If the electromechanical timescale dynamics (~ 1 s) is needed, the constant power input condition $P_{in} = constant$ should be released and the generator-side controls, such as the inertia and rotor speed controls, should be further considered; namely, $P_{in} = P_{in}(t)$. Therefore, the PLL plays a central role on the system dynamics, working as a core in the globe in the figure.

imbalance on the rotor is clear. Here, however, it seems that it is close to the PLL dynamics, which is usually within the electromagnetic timescale. In addition, the power imbalance seemingly has no direct connection with the synchronization state. Our recent study shows that if the electromechanical timescale controllers are considered, the PLL output phase dynamics can be slower and comparable with the rotor dynamics of SG. Hence, the PLL output phase is flexible, relying on the outer controllers and electromechanical devices. In addition, we believe that the PLL output phase can play a similar role with the rotor angle of the SG, and its swing between different renewable devices is dominant. Thus, although the synchronization object has been shifted from the rotor (as a solid physical element) to the PLL (as a soft control element), the physical nature is the same as phase synchronization for any general nonlinear system. In addition, as the objective of PLL is to achieve synchronization between a renewable device with the infinite bus (or between different renewable devices), the synchronization between the terminal voltage or current of a renewable device is dominant, and meanwhile, the synchronization between the terminal voltage phase and the PLL output phase within the device is not. With wide numerical simulations, it has been found that in transient, the PLL self-synchronization (for the PLL input–output phase difference within a certain small range) is always maintained, i.e., $\varphi \approx \varphi_r$, as we have seen in Figs. 6–9.

- (2) For the multi-timescale analysis, in the present study, we have completely ignored the current control loops and treated the transmission line dynamics under the quasi-steady-state assumption. However, the dynamical response of the current control in the VSC can reach up to a few milliseconds, which means that it may be inappropriate to directly neglect the variation of frequency on the transmission lines and loads. For model integrity, the impact of the fast timescale on the system dynamics and the synchronization should be studied in detail.^{70,71} Correspondingly, it is also essential to reveal the properties of dynamic networks and their role in the renewable-dominated power system. On the other hand, for the slow-timescale dynamics, the impact of the generator-side electromechanical timescale controllers should also be evaluated, such as the inertial control and the rotor speed control in Fig. 2.
- (3) Here, we pay close attention to the phase dynamics and the associated angle synchronization phenomenon. Actually, synchronization (rotor-angle) stability, voltage stability, and frequency stability in the traditional power systems commonly occur under different situations. Therefore, their mutual interaction and relation in this new environment should also be investigated.
- (4) For the transient synchronization stability analysis, the system nonlinearity must be considered. Based on the derived dynamical equations for coupled converter systems, they become much more complicated, to be compared with the traditional swing equations of SGs. This naturally brings difficulty for system analysis and calls for new methods.
- (5) Finally, due to the weak over-current and over-voltage capability, there are various protection schemes to prevent damage of power electronic devices during severe fault transient processes, such as crowbar, chopper, emergency pitching control,

etc. Thus, the dynamic behaviors may be characterized by a set of discontinuous hybrid dynamical equations, which leads to difficulty in theoretical analyses. Voltage and current outputs are governed by diverse emergency controllers and switch and/or saturation within multiple timescales, and thus, switched dynamical behavior should be further considered and studied.

ACKNOWLEDGMENTS

This work was partially supported by the National Natural Science Foundation of China under Grant Nos. U22B6008 and 12075091 and the open subject of the State Key Laboratory of Advanced Electromagnetic Engineering and Technology under Grant No. 2021KF003. C. Lin was supported by the National Natural Science Foundation of China under Grant Nos. 12171179 and 11871061 and the Natural Science Foundation of Hubei Province under Grant No. 2020CFB847.

AUTHOR DECLARATIONS

Conflict of Interest

The authors have no conflicts to disclose.

Author Contributions

Rui Ma: Conceptualization (lead); Investigation (lead); Validation (lead); Writing – original draft (lead); Writing – review & editing (lead). **Yayao Zhang:** Validation (supporting); Writing – original draft (supporting); Writing – review & editing (supporting). **Ziqian Yang:** Investigation (supporting); Writing – original draft (supporting); Writing – review & editing (supporting). **Jürgen Kurths:** Writing – original draft (supporting); Writing – review & editing (supporting). **Meng Zhan:** Conceptualization (lead); Investigation (lead); Supervision (lead); Writing – original draft (equal); Writing – review & editing (equal). **Congping Lin:** Funding acquisition (supporting); Supervision (supporting); Writing – review & editing (supporting).

DATA AVAILABILITY

The data that support the findings of this study are available within the article.

APPENDIX: PARAMETERS USED IN THE SIMULATION

Parameters of the electrical network: $f_0 = 50$ Hz (1.0 pu), $\omega_0 = 2\pi f_0$ (1.0 pu), $L_f = 0.1$ pu, and $L_g = 0.5$ pu. Parameters of the controls: (1) DVC: $k_{p,dvc} = 2$, $k_{i,dvc} = 80$. (2) TVC: $k_{p,tvc} = 0.2$, $k_{i,tvc} = 23$. (3) ACC: $k_{p,acc} = 1.3$, $k_{i,acc} = 670$. (4) PLL: $k_{p,pll} = 50$, $k_{i,pll} = 2000$.

REFERENCES

- ¹S. H. Strogatz, *Nonlinear Dynamics and Chaos: With Applications to Physics, Biology, Chemistry, and Engineering* (Westview Press, 2015).
- ²A. S. Pikovsky, M. G. Rosenblum, and J. Kurths, *Synchronization: A Universal Concept in Nonlinear Science* (Cambridge University Press, 2001).
- ³P. Kundur, *Power System Stability and Control* (McGraw-Hill, 1994).
- ⁴P. M. Anderson and A. A. Fouad, *Power System Control and Stability* (The Iowa State University Press, 1994).

- ⁵F. Rodrigues, T. Peron, P. Ji, and J. Kurths, "The Kuramoto model in complex networks," *Phys. Rep.* **610**, 1–98 (2016).
- ⁶D. Witthaut, F. Hellmann, J. Kurths, S. Kettemann, H. Meyer-Ortmanns, and M. Timme, "Collective nonlinear dynamics and self-organization in decentralized power grids," *Rev. Mod. Phys.* **94**, 015005 (2022).
- ⁷P. Kundu, C. Hens, B. Barzel, and P. Pal, "Perfect synchronization in networks of phase-frustrated oscillators," *Europhys. Lett.* **120**, 40002 (2017).
- ⁸Y. Xue, T. Van Cutsem, and M. Ribbens-Pavella, "A simple direct method for fast transient stability assessment of large power systems," *IEEE Trans. Power Syst.* **3**, 400–412 (1988).
- ⁹H.-D. Chiang, C.-C. Chu, and G. Cauley, "Direct stability analysis of electric power systems using energy functions: Theory, applications, and perspective," *Proc. IEEE* **83**, 1497–1529 (1995).
- ¹⁰Y. Sun, J. Ma, J. Kurths, and M. Zhan, "Equal-area criterion in power systems revisited," *Proc. R. Soc. A* **474**, 20170733 (2018).
- ¹¹J. Ma, Y. Sun, X. Yuan, J. Kurths, and M. Zhan, "Dynamics and collapse in a power system model with voltage variation: The damping effect," *PLoS One* **11**, e0165943 (2016).
- ¹²D. Skubov, A. Lukin, and I. Popov, "Bifurcation curves for synchronous electrical machine," *Nonlinear Dyn.* **83**, 2323–2329 (2016).
- ¹³Q. Qiu, R. Ma, J. Kurths, and M. Zhan, "Swing equation in power systems: Approximate analytical solution and bifurcation curve estimate," *Chaos* **30**, 013110 (2020).
- ¹⁴M. Sarkar and S. Gupta, "Synchronization in the Kuramoto model in presence of stochastic resetting," *Chaos* **32**, 073109 (2022).
- ¹⁵B. Schafer and G. Yalcin, "Dynamical modeling of cascading failures in the Turkish power grid," *Chaos* **29**, 093134 (2019).
- ¹⁶A. Motter, S. Myers, M. Anghel, and T. Nishikawa, "Spontaneous synchrony in power-grid networks," *Nat. Phys.* **9**, 191–197 (2013).
- ¹⁷C. Wang, C. Grebogi, and M. Baptista, "Control and prediction for blackouts caused by frequency collapse in smart grids," *Chaos* **26**, 093119 (2016).
- ¹⁸J. Grzybowski, E. Macau, and T. Yoneyama, "On synchronization in power-grids modelled as networks of second-order Kuramoto oscillators," *Chaos* **26**, 113113 (2016).
- ¹⁹P. J. Menck, J. Heitzig, J. Kurths, and H. Joachim Schellnhuber, "How dead ends undermine power grid stability," *Nat. Commun.* **5**, 3969 (2014).
- ²⁰P. Schultz, J. Heitzig, and J. Kurths, "Detours around basin stability in power networks," *New J. Phys.* **16**, 125001 (2014).
- ²¹Y. Yang, T. Nishikawa, and A. E. Motter, "Small vulnerable sets determine large network cascades in power grids," *Science* **358**, eaan3184 (2017).
- ²²M. Rohden, A. Sorge, M. Timme, and D. Witthaut, "Self-organized synchronization in decentralized power grids," *Phys. Rev. Lett.* **109**, 064101 (2012).
- ²³F. Dörfler, M. Chertkov, and F. Bullo, "Synchronization in complex oscillator networks and smart grids," *Proc. Natl. Acad. Sci. U.S.A.* **110**, 2005–2010 (2013).
- ²⁴Z. Yang, R. Ma, S. Cheng, and M. Zhan, "Problems and challenges of power-electronic-based power system stability: A case study of transient stability comparison," *Acta Phys. Sin.* **69**, 103–116 (2020) (in Chinese).
- ²⁵J. Yu, Z. Yang, J. Kurths, and M. Zhan, "Small-signal stability of multi-converter infeed power grids with symmetry," *Symmetry* **13**, 1–25 (2021).
- ²⁶X. He, H. Geng, and G. Mu, "Modeling of wind turbine generators for power system stability studies: A review," *Renew. Sust. Energy Rev.* **143**, 110865 (2021).
- ²⁷Joint NERC and WECC Staff, "900mw fault induced solar photovoltaic resource interruption disturbance report," Technical Report, 2018.
- ²⁸Australian Energy Market Operator, "Black system South Australia," Technical Report, 2016.
- ²⁹National Grid ESO, "Technical report on the events of 9 August 2019," Technical Report, 2019.
- ³⁰Project Group of Global Engineering Fronts of Chinese Academy of Engineering, *Engineering Fronts* (Higher Education Press, 2021), p. 115.
- ³¹H. Pico and B. Johnson, "Transient stability assessment of multi-machine multi-converter power systems," *IEEE Trans. Power Syst.* **34**, 3504–3514 (2019).
- ³²Y. Zhang, C. Zhang, and X. Cai, "Large-signal grid-synchronization stability analysis of pll-based VSCs using Lyapunov's direct method," *IEEE Trans. Power Syst.* **37**, 788–791 (2022).
- ³³Q. Hu, L. Fu, F. Ma, and F. Ji, "Large signal synchronizing instability of PLL-based VSC connected to weak AC grid," *IEEE Trans. Power Syst.* **34**, 3220–3229 (2019).
- ³⁴X. Fu, J. Sun, M. Huang, Z. Tian, H. Yan, H. H.-C. Iu, P. Hu, and X. Zha, "Large-signal stability of grid-forming and grid-following controls in voltage source converter: A comparative study," *IEEE Trans. Power Electron.* **36**, 7832–7840 (2021).
- ³⁵R. Ma, J. Li, J. Kurths, S. Cheng, and M. Zhan, "Generalized swing equation and transient synchronous stability with PLL-based VSC," *IEEE Trans. Energy Convers.* **37**, 1428–1441 (2022).
- ³⁶C. Zhang, X. Cai, A. Rygg, and M. Molinas, "Modeling and analysis of grid-synchronizing stability of a type-IV wind turbine under grid faults," *Int. J. Electr. Power Energy Syst.* **117**, 105544 (2020).
- ³⁷M. Huang, Y. Peng, C. Tse, Y. Liu, J. Sun, and X. Zha, "Bifurcation and large-signal stability analysis of three-phase voltage source converter under grid voltage dips," *IEEE Trans. Power Electron.* **32**, 8868–8879 (2017).
- ³⁸Z. Yang, R. Ma, S. Cheng, and M. Zhan, "Nonlinear modeling and analysis of grid-connected voltage-source converters under voltage dips," *IEEE J. Emerg. Sel. Top. Power Electron.* **8**, 3281–3292 (2020).
- ³⁹R. Ma, Z. Yang, S. Cheng, and M. Zhan, "Sustained oscillations and bifurcations in three-phase voltage source converters tied to AC grid," *IET Renew. Power Gener.* **14**, 3770–3781 (2020).
- ⁴⁰H. Wu and X. Wang, "Design-oriented transient stability analysis of PLL-synchronized voltage-source converters," *IEEE Trans. Power Electron.* **35**, 3573–3589 (2020).
- ⁴¹Z. Zhang, R. Schuerhuber, L. Fickert, K. Friedl, G. Chen, and Y. Zhang, "Domain of attraction's estimation for grid connected converters with phase-locked loop," *IEEE Trans. Power Syst.* **37**, 1351–1362 (2022).
- ⁴²C. Zhang, M. Molinas, Z. Li, and X. Cai, "Synchronizing stability analysis and region of attraction estimation of grid-feeding VSCs using sum-of-squares programming," *Front. Energy Res.* **8**, 1–12 (2020).
- ⁴³J. Hu, X. Yuan, and S. Cheng, "Multi-time scale transients in power-electronized power systems considering multi-time scale switching control schemes of power electronics apparatus," *Proc. CSEE* **39**, 5457–5467 (2019) (in Chinese).
- ⁴⁴J. Hu, B. Wang, W. Wang, H. Tang, Y. Chi, and Q. Hu, "Small signal dynamics of dfig-based wind turbines during riding through symmetrical faults in weak AC grid," *IEEE Trans. Energy Convers.* **32**, 720–730 (2017).
- ⁴⁵A. Sajadi, R. Kenyon, and B.-M. Hodge, "Synchronization in electric power networks with inherent heterogeneity up to 100% inverter-based renewable generation," *Nat. Commun.* **13**, 2490 (2022).
- ⁴⁶Z. Yang, M. Zhan, D. Liu, C. Ye, K. Cao, and S. Cheng, "Small-signal synchronous stability of a new-generation power system with 100% renewable energy," *IEEE Trans. Power Syst.* (published online 2022).
- ⁴⁷X. Zhao, P. Thakurta, and D. Flynn, "Grid-forming requirements based on stability assessment for 100% converter-based Irish power system," *IET Renew. Power Gener.* **16**, 447–458 (2022).
- ⁴⁸C. Breyer, S. Khalili, D. Bogdanov, M. Ram, A. S. Oyewo, A. Aghahosseini, A. Gulagi, A. A. Solomon, D. Keiner, G. Lopez, P. A. Ostergaard, H. Lund, B. V. Mathiesen, M. Z. Jacobson, M. Victoria, S. Teske, T. Pregger, V. Fthenakis, M. Raugi, H. Holtinen, U. Bardi, A. Hoekstra, and B. K. Sovacool, "On the history and future of 100% renewable energy systems research," *IEEE Access* **10**, 78176–78218 (2022).
- ⁴⁹X. Wang, M. G. Taul, H. Wu, Y. Liao, F. Blaabjerg, and L. Harnefors, "Grid-synchronization stability of converter-based resources—An overview," *IEEE Open J. Ind. Appl.* **1**, 115–134 (2020).
- ⁵⁰R. Rosso, X. Wang, M. Liserre, X. Lu, and S. Engelken, "Grid-forming converters: Control approaches, grid-synchronization, and future trends—A review," *IEEE Open J. Ind. Appl.* **2**, 93–109 (2021).
- ⁵¹Q. Jiang and C. Zhao, "Electromagnetic transient synchronization stability issue of grid-connected inverters," *J. Tsinghua Univ.* **21**, 1–14 (2021) (in Chinese).
- ⁵²H. Geng, C. He, Y. Liu, X. He, and M. Li, "Overview on transient synchronization stability of renewable-rich power systems," *High Voltage Eng.* **48**, 3367–3383 (2022) (in Chinese).
- ⁵³Y. Zhang, X. Cai, C. Zhang, J. Lyu, and Y. Li, "Transient synchronization stability analysis of voltage source converters: A review," *Proc. CSEE* **41**, 1687–1701 (2021) (in Chinese).

- ⁵⁴Y. Gu and T. C. Green, "Power system stability with a high penetration of inverter-based resources," *Proc. IEEE* (published online, 2022).
- ⁵⁵Q. Zhong and G. Weiss, "Synchronverters: Inverters that mimic synchronous generators," *IEEE Trans. Ind. Electron.* **58**, 1259–1267 (2011).
- ⁵⁶V. Gevorgian and B. O'Neill, "Advanced grid-friendly controls demonstration project for utility-scale PV power plants," Technical Report, National Renewable Energy Laboratory, 2016.
- ⁵⁷E. Rokrok, T. Qoria, A. Bruyere, B. Francois, and X. Guillaud, "Transient stability assessment and enhancement of grid-forming converters embedding current reference saturation as current limiting strategy," *IEEE Trans. Power Syst.* **37**, 1519–1531 (2021).
- ⁵⁸X. Zha, M. Huang, Y. Liu, and Z. Tian, "An overview on safe operation of grid-connected converters from resilience perspective: Analysis and design," *Int. J. Electr. Power Energy Syst.* **143**, 108511 (2022).
- ⁵⁹A. Yazdani and R. Iravani, *Voltage-Sourced Converters in Power Systems: Modeling, Control, and Applications* (John Wiley & Sons, 2010).
- ⁶⁰X. Yuan, S. Cheng, and J. Hu, "Multi-time scale voltage and power angle dynamics in power electronics dominated large power systems," *Proc. CSEE* **36**, 5145–5154 (2016) (in Chinese).
- ⁶¹R. Ma, Q. Qiu, J. Kurths, and M. Zhan, "Fast-slow-scale interaction induced parallel resonance and its suppression in voltage source converters," *IEEE Access* **9**, 90126–90141 (2021).
- ⁶²M. Zarif Mansour, S. Me, S. Hadavi, B. Badrzadeh, A. Karimi, and B. Bahrani, "Nonlinear transient stability analysis of phased-locked loop based grid-following voltage source converters using Lyapunov's direct method," *IEEE J. Emerg. Sel. Top. Power Electron.* **10**, 2699–2709 (2022).
- ⁶³Y. Kang, X. Lin, Y. Zheng, X. Quan, J. Hu, and X. Yuan, "The static stable-limit and static stable-working zone for single-machine infinite-bus system of renewable-energy grid-connected converter," *Proc. CSEE* **40**, 4506–4515 (2020) (in Chinese).
- ⁶⁴L. Xiong, F. Zhuo, F. Wang, X. Liu, Y. Chen, M. Zhu, and H. Yi, "Static synchronous generator model: A new perspective to investigate dynamic characteristics and stability issues of grid-tied PWM inverter," *IEEE Trans. Power Electron.* **31**, 6264–6280 (2016).
- ⁶⁵Z. Yang, J. Yu, J. Kurths, and M. Zhan, "Nonlinear modeling of multi-converter systems within DC-link timescale," *IEEE J. Emerg. Sel. Top. Circuits Syst.* **11**, 5–16 (2021).
- ⁶⁶C. Shen, Z. Shuai, Y. Shen, Y. Peng, X. Liu, Z. Li, and Z. J. Shen, "Transient stability and current injection design of paralleled current-controlled VSCs and virtual synchronous generators," *IEEE Trans. Smart Grid* **12**, 1118–1134 (2021).
- ⁶⁷X. He and H. Geng, "Transient stability of power systems integrated with inverter-based generation," *IEEE Trans. Power Syst.* **36**, 553–556 (2021).
- ⁶⁸X. Fu, M. Huang, S. Pan, and X. Zha, "Cascading synchronization instability in multi-VSC grid-connected system," *IEEE Trans. Power Electron.* **37**, 7572–7576 (2022).
- ⁶⁹X. He and H. Geng, "Synchronization stability analysis and enhancement of grid-tied multi-converter systems," in *2020 IEEE Industry Applications Society Annual Meeting* (IEEE, 2020), pp. 1–8.
- ⁷⁰Y. Ji, W. He, S. Cheng, J. Kurths, and M. Zhan, "Dynamic network characteristics of power-electronics-based power systems," *Sci. Rep.* **10**, 1–16 (2020).
- ⁷¹X. Yang, R. Ma, and M. Zhan, "Dynamic and static network analysis and power transmission characteristics of power system oscillations," in *Proceedings of CSEE* (to be published) (2022) (in Chinese); available at <https://kns.cnki.net/kcms/detail/11.2107.TM.20220926.1758.018.html>.